An ALS-linked mutation in TDP-43 disrupts normal protein interactions in the motor neuron response to oxidative stress

Emily Feneberg[a], David Gordon[a], Alexander G. Thompson[a], Mattéa J. Finelli[a], Ruxandra Dafinca[a], Ana Candalija[a], Philip D. Charles[b], Imre Mäger[c], Matthew J. Wood[c], Roman Fischer[b], Benedikt M. Kessler[b], Elizabeth Gray[a], Martin R. Turner[a,*], Kevin Talbot[a,d,*]

[a] Nuffield Department of Clinical Neurosciences, University of Oxford, Oxford OX3 9DU, United Kingdom
[b] Target Discovery Institute, Nuffield Department of Medicine, University of Oxford, Oxford OX3 7FZ, United Kingdom
[c] Department of Paediatrics, Medical Sciences Division, University of Oxford, Oxford OX3 9DU, United Kingdom
[d] Lead Contact

ARTICLE INFO

ABSTRACT

TDP-43 pathology is a key feature of amyotrophic lateral sclerosis (ALS), but the mechanisms linking TDP-43 to altered cellular function and neurodegeneration remain unclear. We have recently described a mouse model in which human wild-type or mutant TDP-43 are expressed at low levels and where altered stress granule formation is a robust phenotype of TDP-43$^{M337V/-}$ expressing cells. In the present study we use this model to investigate the functional connectivity of human TDP-43 in primary motor neurons under resting conditions and in response to oxidative stress. The interactome of human TDP-43^{WT} or TDP-43^{M337V} was compared by mass spectrometry, and gene ontology enrichment analysis identified pathways dysregulated by the M337V mutation. We found that under normal conditions the interactome of human TDP-43^{WT} was enriched for proteins involved in transcription, translation and poly(A)-RNA binding. In response to oxidative stress, TDP-43^{WT} recruits proteins of the endoplasmic reticulum and endosomal-extracellular transport pathways, interactions which are reduced in the presence of the M337V mutation. Specifically, TDP-43^{M337V} impaired protein-protein interactions involved in stress granule formation including reduced binding to the translation initiation factors Poly(A)-binding protein and Eif4a1 and the endoplasmic reticulum chaperone Grp78. The M337V mutation also affected interactions involved in endosomal-extracellular transport and this this was associated with reduced extracellular vesicle secretion in primary motor neurons from TDP-43$^{M337V/-}$ mice and in human iPSCs-derived motor neurons. Taken together, our analysis highlights a TDP-43 interaction network in motor neurons and demonstrates that an ALS associated mutation may alter the interactome to drive aberrant pathways involved in the pathogenesis of ALS.

1. Introduction

The presence of ubiquitinated and phosphorylated aggregates of the 43 kDa transactive response DNA-binding protein (TDP-43) in the cytoplasm of neurons is one of the defining pathological hallmark of amyotrophic lateral sclerosis (ALS) and approximately 50% of cases of frontotemporal dementia (FTD) (Neumann et al., 2006). TDP-43 pathology is also now recognised as a significant factor in at least 25% of cases of late-onset cognitive decline designated as 'limbic-predominant age-related TDP-43 encephalopathy' (LATE) and in chronic traumatic encephalopathy (McKee et al., 2016; Nelson et al., 2019). The distribution of TDP-43 pathology within the central nervous system in ALS

correlates well with disease burden, although the mechanisms leading to cell death remain unclear (Brettschneider et al., 2013; Lee et al., 2011).

TDP-43 is a ubiquitously expressed heterogeneous nuclear ribonucleoprotein (hnRNP) containing two highly conserved RNA-recognition motifs (RRM) and a C-terminal glycine-rich domain (Kato et al., 2012; Ou et al., 1995). Which of its diverse functions are key in ALS pathogenesis remains unclear. The C-terminal region of TDP-43 is important in its interaction with other proteins to regulate key cellular functions such as alternative splicing and translation (Ayala et al., 2011; Buratti and Baralle, 2008; Buratti et al., 2005; Ling et al., 2013), and in mediating liquid–liquid phase transitions, which are important for the

biogenesis of membraneless organelles such as stress granules. However, this 'low-complexity domain' also renders TDP-43 prone to misfolding and aggregation (Conicella et al., 2016; Harrison and Shorter, 2017). Notably, ALS-associated mutations in TDP-43 are consistently located in the C-terminus, suggesting that it mediates protein-protein interactions critical to ALS pathogenesis (Sreedharan et al., 2008).

We recently described a mouse model with low level expression of human TDP-43 from a single copy stably-integrated BAC genomic construct containing human wild-type TDP-43 or C-terminal mutated TDP-43 (M337V) with a C-terminal fluorescent protein tag (YPet) (Gordon et al., 2019). Heterozygous TDP-43 $^{M337V/-}$ mice showed motor deficits at 12 months and reduced survival at 2 years, compared to non-transgenic mice. Importantly, these phenotypes were observed in the absence of TDP-43 insoluble aggregates, suggesting it is relevant model in which to study early pathological events upstream of protein aggregation. In motor neurons differentiated from TDP-43$^{M337V/-}$ BAC-transgenic mouse embryonic stem-cells (mESC) oxidative stress, an important driver of neurodegeneration, led to a robust phenotype of reduced stress granule formation (Gordon et al., 2019; Shaw et al., 1995).

A number of proteomic studies have investigated TDP-43 interactors, although these have generally not been conducted in primary motor neurons with disease relevant phenotypes, and were lacking a direct comparison between the wild-type protein and a C-terminal mutant version of TDP-43, which may limit their relevance to ALS pathogenesis (Blokhuis et al., 2016; Freibaum et al., 2010; Li et al., 2016; Ling et al., 2010). The aim of the current study was therefore to take advantage of the more physiological level of expression in this model to investigate the functional connectivity of human TDP-43^{WT} in differentiated motor neurons at rest and in response to oxidative stress. Hypothesising that TDP-43^{M337V} mediates altered protein-protein interactions that are linked to ALS pathophysiology, we then identified specific pathways disrupted by the mutation and linked these to reproducible cellular phenotypes in primary motor neurons.

2. Results

2.1. Low-level expression of human TDP-43$^{M337V/-}$ in primary motor neuron cultures leads to reduced survival in response to oxidative stress

Mouse ES-cell derived motor neurons expressing YPet-tagged human wild-type (TDP-43^{WT}) or M337V mutant (TDP-43^{M337V}) TDP-43 were lysed after 2 days of motor neuron specification, at which timepoint all cultures were also assessed for consistency. We observed no obvious alteration in cell division or viability between genotypes. Immunohistochemistry confirmed that 73% of total cells co-expressed the neuronal marker Tuj1 and the early motor neuronal marker Islet1 ($p = 0.196$) (Fig. 1A and B), and over 70% of total cells co-expressed Tuj1 and the mature motor neuronal marker ChAT ($p = 0.557$, supplementary Fig.1). Immunoblotting showed human YPet-tagged TDP-43^{WT} or TDP-43^{M337V} protein (72 kDa) at 0.17 and 0.14 times the level of mouse endogenous Tdp-43 (43 kDa) ($p = 0.99$, respectively). Endogenous mouse Tdp-43 protein levels were equivalent between (BAC)-transgenic and non-transgenic motor neuron lysates ($p = 0.89$) (Fig. 1C and D).

Given our previous observation of altered stress granule dynamics in TDP-43^{M337V} mice, we also assessed motor neuron cultures under conditions sufficient to induce stress granule formation by treating cells with 0.5 mM NaAsO$_2$ for 60 min. Importantly, the mESC-derived TDP-43$^{M337V/-}$ motor neurons did not show mislocalization of human YPet-tagged TDP-43 in basal or stress conditions, and thus any interactome changes are not purely a consequence of a shift to cytoplasmic localization of human TDP-43^{M337V} (Fig. 1E). NaAsO$_2$ treatment was associated with the expression of cleaved-caspase 3 in less than 20% of cells in either genotype ($p = 0.088$, Fig. 1F). Significantly reduced survival of TDP-43$^{M337V/-}$ compared to TDP-43$^{WT/-}$ motor neurons was

observed at 4 h after 60 min of NaAsO$_2$ treatment ($p = 0.0009$, Fig. 1G).

2.2. An ALS-associated C-terminal mutation alters the normal interactome of human TDP-43

To determine the human TDP-43 interactome, wild-type or mutant TDP-43 and their interactors were immunoprecipitated using GFP antibody-coated beads from motor neuron lysates $+/-$ 60 min of 0.5 mM NaAsO$_2$. The efficiency of the immunoprecipitation was confirmed by immunoblotting and detection of the YPet-tagged TDP-43. GFP-immunoprecipitation from equal input amounts led to specific enrichment of YPet-tagged TDP-43 at 72 kDa with complete depletion from the supernatant, which contained the residual endogenous Tdp-43 at 43 kDa (Fig. 2A).

Across all GFP-immunoprecipitated samples, a total of 534 proteins were co-immunoprecipitated and identified by mass spectrometry. As expected, the YPet bait was detected equally in all samples. While some proteins were equally abundant between genotypes, specific proteins were differentially abundant in motor neurons expressing either TDP-43^{WT} or TDP-43^{M337V}. Hierarchical clustering by genotype showed a cluster of proteins with missing ion abundances in TDP-43^{M337V} samples (Fig. 2B). To take account of putative interactors that were specific to either genotype, we determined the presence or absence of an interactor using peptide spectral counts to avoid the imputation of missing ion abundances (Supplementary tables 1 and 2). This revealed 249 putative interactors that were present in the TDP-43^{WT} interactome, but absent in the TDP-43^{M337V} interactome, which was also reflected in a higher total spectral count number in all three replicate samples for TDP-43^{WT} ($p = 0.036$) (Fig. 2C). In contrast, 43 putative interactors were specific to the TDP-43^{M337V} interactome, with a higher number of total spectral counts per sample compared to TDP-43^{WT} ($p = 0.026$). Similar findings were observed in the presence of oxidative stress, where 203 proteins were specific for TDP-43^{WT} and 26 proteins specific for TDP-43^{M337V}, with a significantly reduced total number of total spectral counts for specific interactors (both $p = 0.004$). The number of putative interactors of TDP-43^{M3337V} was therefore reduced (Chi-square $p = 0.03$), suggesting that the mutation is likely to have a significant effect on the normal function of TDP-43, in addition to promoting aberrant protein-protein interactions which are potentially toxic. Individual TDP-43^{WT} or TDP-43^{M337V} interactors of particular interest in basal or stress conditions and their abundance by spectral counts are given in Fig. 2D. Our data shows considerable overlap with previous TDP-43 wild-type interactome studies (Supplementary Fig. 2) (Freibaum et al., 2010; Ling et al., 2010). 62% of nuclear and 78% of cytoplasmic interactors were in common with the study of Freibaum et al. Compared to the most stringent interactome study that used absolute quantification with affinity purification mass spectrometry (AP-MS), TDP-43^{WT} in our study had 50% of nuclear interactors and 36% of other interactors in common (Ling et al., 2010). For the TDP-43^{M337V} interactome no previous mass spectrometry is available for direct comparison, but in line with our results, overlap with the wild-type interactome reported in previous studies was greatly reduced (23%, 27% and 28% respectively).

2.3. Mutant TDP-43 induces a shift towards acquired interactions in pathways linked to ALS pathogenesis

Gene ontology (GO) enrichment analyses of the putative interactors specific for either TDP-43^{WT} or TDP-43^{M337V} demonstrated differences in their functional role. Proteins bound to TDP-43^{WT} were enriched for terms including 'transcription' (odds ratio, OR 5.5, $p = 0.03$), 'translation' (OR 3.2, $p = 0.02$), 'ribosome formation' (OR 1.8, $p = 0.003$), and 'Poly(A)-RNA binding' (OR 1.4, $p = 0.004$) (Fig. 3A). In response to NaAsO$_2$ stress treatment the TDP-43^{WT} interactome gained 92 new interactors (Supplementary Fig. 3A), with a shift towards proteins
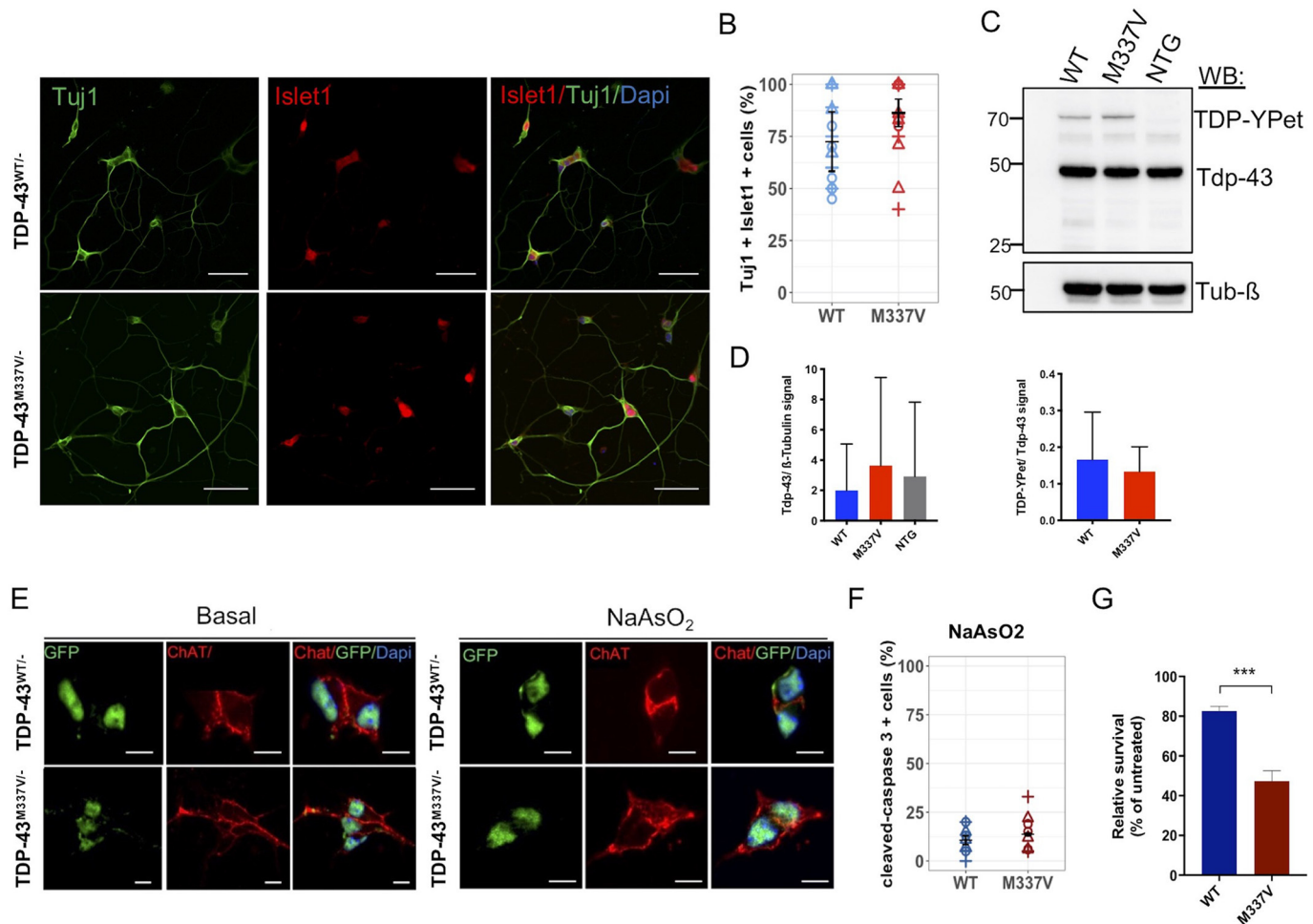
Fig. 1. Low-level expression of human TDP-43$^{M337V/-}$ in (BAC)-transgenic MNs leads to reduced survival in response to oxidative stress.
A Immunostaining for Islet1 and Tuj1 in TDP-43$^{WT/-}$ and TDP-43$^{M337V/-}$ cell lines (scale bar 50 μm). B Quantification of Tuj1 and Islet1 positive cells between genotypes ($p = 0.196$) C Immunoblotting with anti-TDP-43 full-length antibody shows absent human YPet-tagged TDP-43 at 72 kDa in non-transgenic (NTG) cell lysates. D Quantification of immunoblots shows mouse Tdp-43 levels at 43 kDa ($p = 0.89$, one-way ANOVA) and low expression of human TDP-YPet levels ($p = 0.99$). E TDP-YPet was retained in the nucleus of ChAT positive MNs $+/-$ 0.5 mM NaAsO$_2$ treatment (scale bar 10 μm). F Quantification of cleaved-caspase 3 positive cells after 1 h NaAsO$_2$ treatment between genotypes ($p = 0.088$). G Reduced survival in TDP-43$^{M337V/-}$ MNs after 1 h NaAsO$_2$ treatment (***$p = 0.001$).
$N = 62$–124 MNs from three independent differentiations; unpaired t-test; TDP-43$^{WT/-}$ (blue), TDP-43$^{M337V/-}$ (red), symbols ($+$,o,∇) represent number of positive stained cells per field and differentiation. Data are represented as mean $\pm$ SD. Abbreviations: DAPI, 40,6-Diamidino-2-Phenylindole; MNs, motor neurons. (For interpretation of the references to colour in this figure legend, the reader is referred to the web version of this article.)

enriched for terms including 'endoplasmic reticulum' (OR 4.5, $p = 0.02$), 'calcium binding' (OR 3.5, $p = 0.001$) and 'endosomal transport and extracellular exosome' (OR6.1, $p = 0.03$ and OR 1.2, $p = 0.04$) (Fig. 3B). Network analysis confirmed the connectivity of proteins involved in transcription and ribosome formation in basal conditions in TDP-43^{WT} samples, and again demonstrated a clear shift towards protein-protein interactions involved in endosomal-exosomal transport in response to oxidative stress (Fig. 3C and supplementary tables 3 and 4). This suggests potentially distinct condition-dependent functions of TDP-43^{WT} in motor neurons, with a predominant role in DNA/RNA metabolism in basal conditions and a shift in function towards intracellular trafficking in response to stress.

In contrast, the TDP-43^{M337V} interactome in basal conditions was enriched for different GO terms including 'protein folding' (OR 13.3, $p = 0.006$) and 'filamin binding' (OR 13.3, $p = 0.005$) (Fig. 3A). Interestingly, complexes of the dihydropyrimidinase-related proteins, DPYSL1 (Crmp1) and DPYSL3, were highly abundant in the TDP-43^{M337V} interactome (Supplementary table 1 and 2). These proteins are known to be modified in neurodegeneration and are involved in several ALS-associated pathways including axonal transport, glutamate excitotoxicity and oxidative stress (Blasco et al., 2013). Importantly, in

response to stress the TDP-43^{M337V} interactome revealed significant GO terms distinct from those seen with TDP-43^{WT}, with high odds ratios for protein ubiquitination (OR 28, $p = 0.001$), protein homo-oligomerization (OR 50, $p = 0.0001$) and endosomal to lysosomal transport (OR 8, $p = 0.02$) (Fig. 3B).

In comparison, GO enrichment of the shared background proteome of both genotypes showed terms for common cellular components such as the cytosolic skeleton, myelin sheath and ribosomal subunits (Supplementary Fig. 3B). Together this indicates that the M337V mutation disturbs the normal TDP-43 interactome in a way that is likely to affect its downstream function, with a shift towards pathways that have been previously established to have a role in ALS pathogenesis.

2.4. Protein interactions underlying translation and stress response pathways are disrupted by the M337V mutation

Our mass spectrometry data analysis identified TDP-43^{WT} binding proteins important for translation and the cellular response to stress. Given the important role of Pabpc in both protein translation, but also as a component of stress granules, we next specifically focused on investigating the interaction between Pabpc and TDP-43.
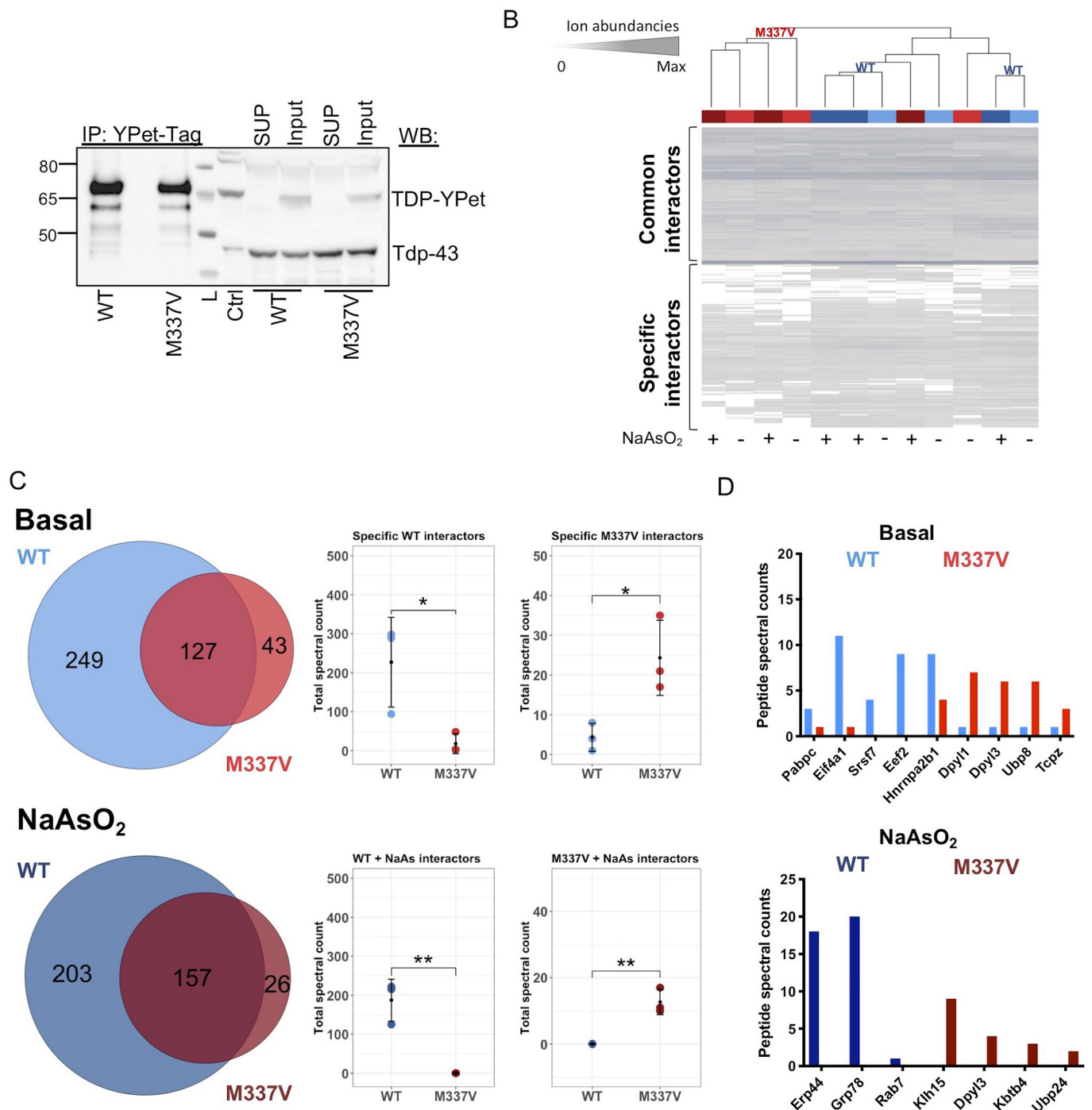
**Fig. 2.** The TDP-43 interactome is altered by the C-terminal TDP-43 mutation.

A Immunoblotting with anti-TDP-43 full-length antibody shows enrichment of human YPet-tagged TDP-43^{WT} and TDP-43^{M337V} at 72kDA after IP. B Hierarchical cluster of protein abundance analysed by LC-MS/MS from Co-IPs across TDP-43^{WT} (blue), TDP-43^{WT} + NaAsO$_2$ (dark blue), TDP-43^{M337V} (red) and TDP-43^{M337V} + NaAsO$_2$ (dark red) samples (n = 3 independent differentiations per sample). C Venn diagrams show the total number of proteins identified by spectral counting in the TDP-43^{WT} or TDP-43^{M337V} interactome (top) and the NaAsO$_2$ treated interactomes (bottom) with a reduction of proteins identified for TDP-43^{M337V}. The total spectral counts of the specific TDP-43^{WT} or TDP-43^{M337V} (*p = 0.036 and p = 0.026), and TDP-43^{WT} + NaAsO$_2$ or TDP-43^{M337V} + NaAsO$_2$ interactors (**, both p = 0.004) are higher; unpaired t-test. D Examples of proteins bound to TDP-43^{WT}, TDP-43^{M337V} or both in basal and stress conditions. Data are represented as mean ± SD. Abbreviations: IP, Immunoprecipitation; MN, motor neuron. (For interpretation of the references to colour in this figure legend, the reader is referred to the web version of this article.)

Co-immunoprecipitation experiments were performed from differentiated mouse motor neuron lysates, which showed that the normal TDP-43^{WT} and Pabpc interaction, is reduced in TDP-43^{M337V} motor neurons under basal (p = 0.049) and NaAsO$_2$ stress (p = 0.047) conditions (Fig. 4A), while protein input levels were similar in both conditions (p = 0.93) and genotypes (basal p = 0.97, stress p = 0.9). In line with the existing literature this interaction was not directly affected by the M337V mutation when overexpressed in HEK293T cells (Supplementary Fig. 4A). However, the interaction was abrogated by RNase treatment (p = 0.045) (Supplementary Fig. 4B). This therefore suggests
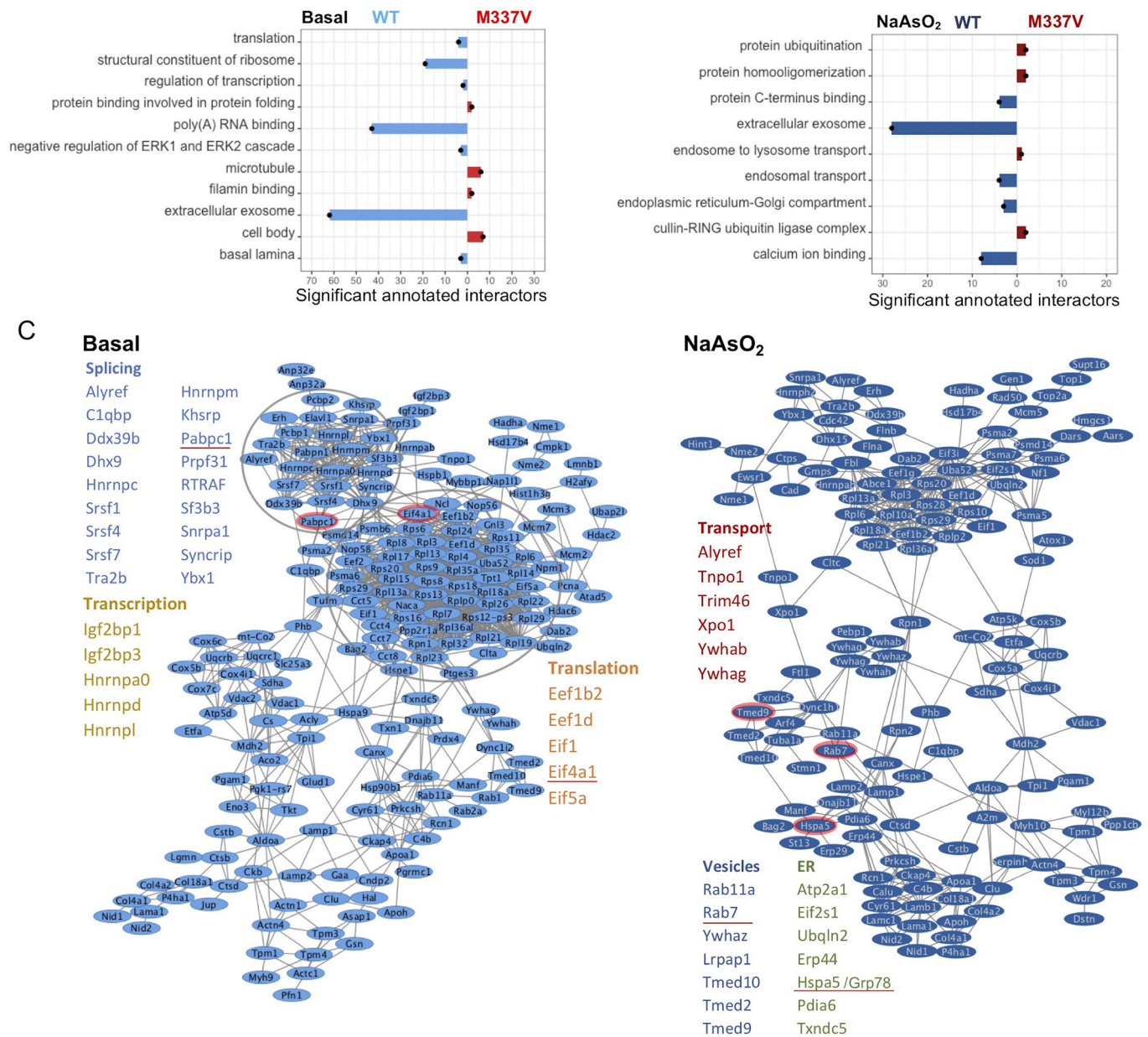
Fig. 3. The physiological function of TDP-43 demonstrated by human TDP-43[WT] interactors is disturbed by the M337V mutation and reveals ALS associated pathways.

A-B Gene Ontology enrichment analysis for significant terms ($p < 0.05$, Fisher's exact test) by number of annotated interactors from the human TDP-43[WT] interactome (blue) and TDP-43[M337V] (red) interactome (a) and in response to 60 min of 0.5 mM NaAsO$_2$ treatment (b). C Protein-protein interaction network analysis of TDP-43[WT] shows a cluster of interactions for proteins involved in transcription and splicing, ribosome formation and translation, (left); in response to stress those clusters resolve (right), while interactions of the endosomal-exosomal pathway form. Pabpc, Eif4a1, Grp78 (synonym name Hspa5) and Tmed9, Rab7 are indicated by red circles. (For interpretation of the references to colour in this figure legend, the reader is referred to the web version of this article.)

that the changes in the TDP-43[M337V] interactome in our model may involve motor neuron specific RNA dependent protein interactions, including translational proteins such as Pabpc.

To extend these observations to other interactors affected by the M337V mutation and involved in RNA processing, we investigated Eif4a1, a subunit of the Eif4f translation initiation factor complex acting upstream of the binding of Pabpc to RNA, and independently associated with stress granule assembly (Kimball et al., 2003). By mass spectrometry we found Eif4a1 to be highly abundant in the TDP-43[WT] interactome under basal conditions, but deficient in the TDP-43[M337V] interactome (Fig. 2D). Co-immunoprecipitation of Eif4a1 and

immunoblotting confirmed the TDP-43[WT] and Eif4a1 interaction and a reduction in interaction of Eif4a1 with TDP-43[M337V] ($p = 0.041$), while total protein levels of Eif4a1 were similar between genotypes ($p = 0.487$) (Fig. 4B).

Next, we looked at differences in TDP-43 interactions in direct response to oxidative stress. Grp78 was shown to be a specific TDP-43[WT] interactor with significantly increased ion abundances compared to TDP-43[M337V] by mass spectrometry ($p = 0.015$) (Fig. 2D). It has an important role in the correct folding and degradation of proteins and regulates the unfolded protein response of the endoplasmic reticulum. By co-immunoprecipitation we confirmed the TDP-43[WT] and Grp78
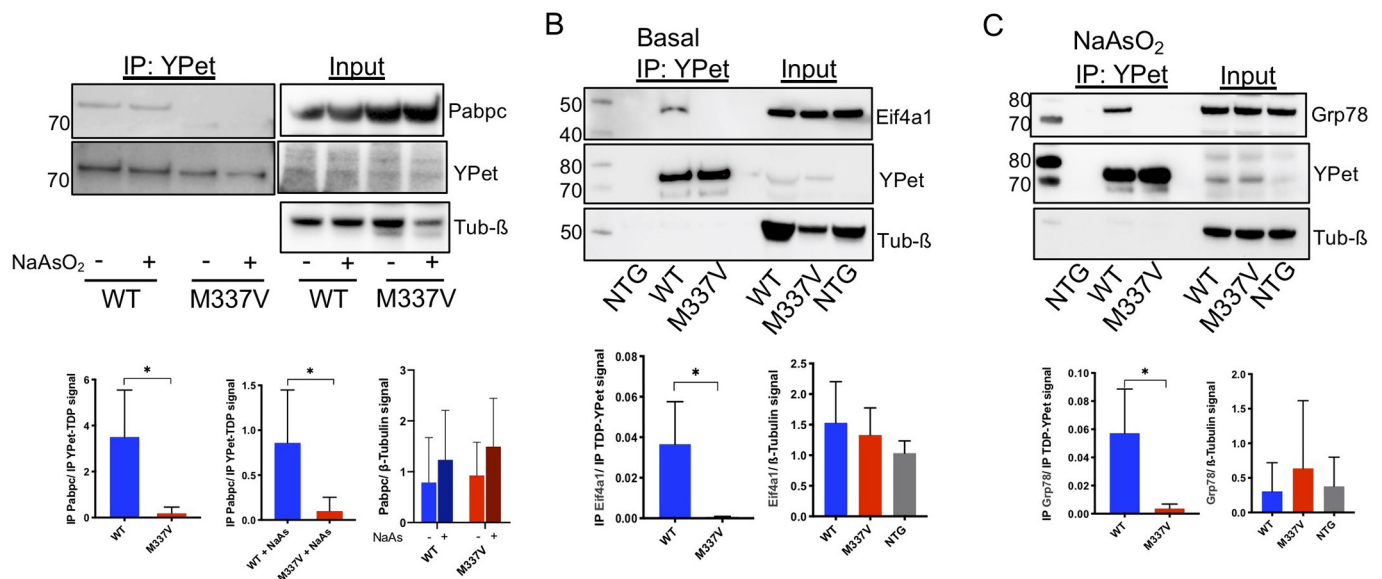
Fig. 4. Protein interactions of human wild-type TDP-43 are disrupted by the C-terminal mutation.
a Co-IP of human YPet-tagged TDP-43 from mouse MN lysates. Immunoreactivity of mouse Pabpc at 75 kDa is reduced in TDP-43^{M337V} +/− NaAsO$_2$ IPs. Immunoreactivity of TDP-YPet at 72 kDa confirms efficiency of the IP. Co-IPs showing Pabpc levels relative to normalized TDP-YPet in TDP-43^{M337V} compared to TDP-43^{WT} in basal (*p = 0.049, unpaired t-test) (n = 3 differentiations) and after 60 min of 0.5 mM NaAsO$_2$ treatment (n = 4 differentiations) (*p = 0.047, unpaired t-test). Pabpc levels are unaltered in MN input lysates +/-NaAsO$_2$ (p = 0.927) and between genotypes (basal, p = 0.97; stress p = 0.9; two-way ANOVA). B Eif4a1 co-immunoprecipitates with TDP-43^{WT} at 48 kDa in basal conditions. C Grp78 co-immunoprecipitation with TDP-43^{WT} or TDP-43^{M337V} in stress conditions. Grp78 levels are unaltered in MN input lysates between genotypes (p = 0.84, one-way ANOVA). B and C N = 3 independent differentiations. Data are represented as mean ± SD. Abbreviations: Co-immunoprecipitations, Co-IP; MNs, motor neurons; IP, Immunoprecipitation, L, Ladder.

interaction and a reduction in interaction of Grp78 with TDP-43^{M337V} after stress treatment (p = 0.043), while input levels of Grp78 were similar between motor neuron lysates (p = 0.84) (Fig. 4C).

Stress granules are RNA-containing cytoplasmic foci formed through liquid-liquid phase separation and are enriched for low complexity domain-containing proteins, including TDP-43 and Pabpc (Colombrita et al., 2009). We previously showed in primary embryonic spinal neurons derived from TDP-43$^{M33V/−}$ mice that fewer Pabpc-positive stress granules were detected in response to 60 min of NaAsO$_2$ treatment (Gordon et al., 2019). We confirmed that the mESC-derived motor neurons used in this study reproduced this phenotype and that stress granules in TDP-43$^{M337V/−}$ motor neurons are smaller (Fig. 5). This study of an ALS associated mutation in a cellular model therefore

suggests that alterations in the interactome of mutant TDP-43 are associated with altered stress granule response to oxidative stress. However, further work would be required to demonstrate a precise mechanistic link for differentially interacting proteins in stress granule assembly.

2.5. M337V mutant TDP-43 disrupts endosomal-exosomal protein pathways and impairs extracellular vesicle secretion

A number of previous studies have provided evidence of a link between endovesicular recycling pathways and ALS, either in the context of autophagy, exosome secretion or axonal vesicular transport (Aoki et al., 2017; Sleigh et al., 2020). Knock-down of TDP-43 also has a
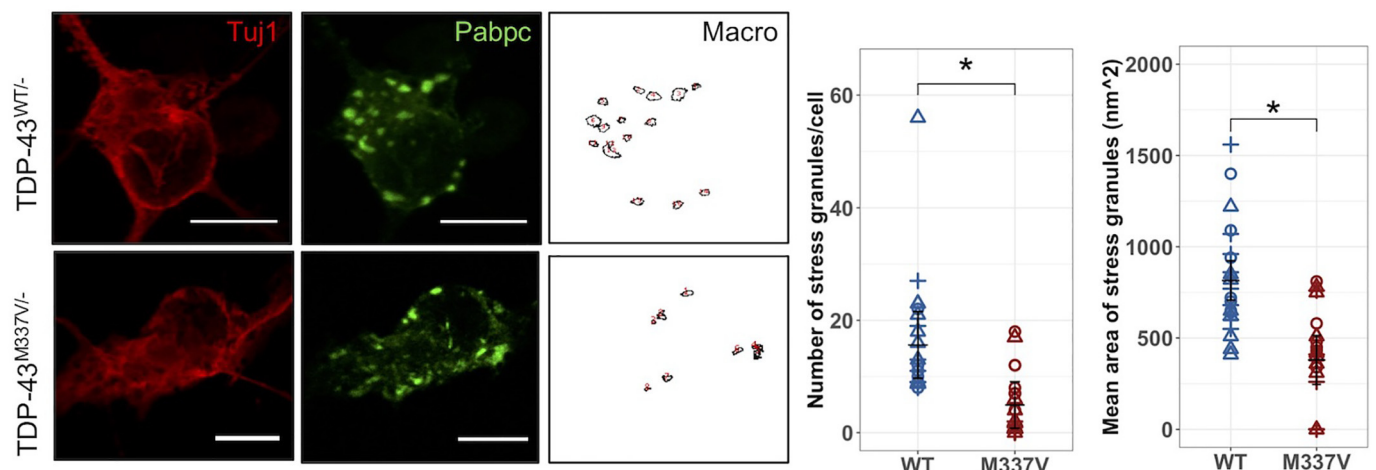
Fig. 5. Poly(A)-binding protein positive stress granule formation is dysregulated in TDP-43$^{M337V/−}$ ESC-derived motor neurons.
Immunostaining of Tuj1- and Pabpc-positive neurons treated for 60 min with 0.5 mM NaAsO$_2$ for automated macro analysis to assess stress granules per cell. Scale bar 10 μm. Quantification shows the number and average area (nm^2) of stress granules per neuron are reduced in human TDP-43$^{M337V/−}$ neurons (both *p = 0.019 and p = 0.013, unpaired t-test). N = 23–25 cells from three independent differentiations. Data are represented as mean ± SD.

direct impact on endosomal trafficking (Schwenk et al., 2016). In our detailed proteomic data, the TDP-43^{WT} interactome is also highly enriched in proteins of the endosomal-exosomal pathway, including proteins that target endosomal trafficking towards extracellular secretion. In contrast, the TDP-43^{M337V} interactome showed a shift towards protein interactors regulating endosomal-lysosomal degradation through interaction with VPS41 (Supplementary table 2). Tmed9 and Rab7-GTPase are putative interactors of TDP-43^{WT} (in the context of NaAsO$_2$ treatment) involved in the extracellular-exosome pathway. There is evidence of weak Tmed9 binding to TDP-43^{WT} by co-immunoprecipitation, with reduced immunoreactivity with TDP-43^{M337V}, but this decrease did not reach statistical significance (p = 0.12) (Supplementary Fig. 5) and we could not confirm an interaction of rab7-GTPase to TDP-43^{WT} or TDP-43^{M337V} by immunoblotting. However, given that Tmed9 and rab7-GTPase were low abundancy proteins in the TDP-43^{WT} + NaAsO$_2$ interactome among 60 other significant proteins involved in extracellular-exosome secretion, we therefore asked if we can observe a direct phenotypic alteration in extracellular vesicle secretion.

Culture medium was collected from equal quantities of plated mouse motor neurons (p = 0.372, supplementary table 5), and the number of extracellular vesicles were quantified by nanoparticle tracking analysis (NTA) following ultrafiltration liquid chromatography. Under basal conditions, no difference in the total number of extracellular vesicles recovered per ml of conditioned media was detectable between genotypes (p = 0.56, Fig. 6a) and between (BAC)-transgenic and non-transgenic mouse motor neurons (p = 0.71, Fig. 6f). However, after 60 min of NaAsO$_2$ stress treatment, a reduction in the number of vesicles was seen in conditioned media from TDP-43$^{M337V/-}$ cells, suggesting that the M337V mutation affects extracellular vesicle secretion (p = 0.048). By NTA of concentrated extracellular vesicle peak fractions we demonstrated that the size distribution in both genotypes is characteristic of a mixed population of vesicles. Vesicles in the size range from 40 to 100 nm are typically exosomes arising from endosomal pathways and the EV peak at 85 nm is decreased for TDP-43$^{M337V/-}$ MNs + NaAsO$_2$ and the area under the curve for exosomes (40–100 nm) and a mixed population of EVs (100–200 nm) (*p = 0.02 and **p = 0.004) (Fig. 6b) (Thery et al., 2006).

To verify that this finding was not limited to a model in which human TDP-43 is expressed in the mouse context, we extended our observations to human iPSC-derived motor neurons. In response to NaAsO$_2$ treatment a reduction in the total number of vesicles of 40–100 nm and 100–200 nm, representing exosomes and extracellular vesicles, was observed in conditioned media from iPSC-derived MNs from an ALS patient with the M337V mutation compared to controls (p = 0.049, Fig. 6c-d). Extracellular vesicle fractions were confirmed by immunoblotting with antibodies against Alix, Tsg101 and Flotillin-1, as well as negative markers of the endoplasmic reticulum, mitochondria and nucleus. The presence, size and morphology of vesicles were further confirmed by transmission electron microscopy (Fig. 6e). These results suggest that extracellular vesicle formation or release is impaired in human and mouse motor neurons by TDP-43^{M337V} through disruption of elements of the wild-type TDP-43 interactome in response to cellular stress.

3. Discussion

A major challenge in neurodegenerative disease is to link cellular phenotypes in model systems directly with the molecular mechanisms driving loss of homeostasis and cell failure. Despite a large number of in vitro and in vivo studies based on TDP-43 models, the mechanisms whereby mutations in *TARDBP* lead to ALS remain uncertain.

Most interactomes are derived from wild-type TDP-43 expressed in non-motor neuron models that do not show an ALS-related phenotype (Blokhuis et al., 2016; Freibaum et al., 2010; Ling et al., 2010). The key question of how ALS-determining mutations are tolerated for long

periods before triggering motor neuron degeneration requires interactome models in which TDP-43 overexpression itself is not toxic and which are relevant for ALS pathology. In this study we have taken advantage of a transgenic mouse model of ALS, in which the wild-type and the mutant TDP-43 genomic construct is site-specifically integrated as a single copy, to drive human TDP-43 from its native promoter throughout the differentiation process of motor neurons (Gordon et al., 2019). Affinity purification of epitope-tagged TDP-43 allowed us to link mutant-specific alterations in the TDP-43 interactome with the phenotypic alterations we observed in mutant TDP-43 motor neurons.

3.1. M337V mutation disturbs the normal TDP-43 interactome

Our data demonstrate that the highly functional TDP-43 interactome in motor neurons is disturbed by the presence of the M337V mutation. First, we confirmed previous findings that, under basal conditions, human TDP-43^{WT} interacts with proteins involved in transcription, splicing and translation (Freibaum et al., 2010). We then showed that TDP-43^{M337V} binding to previously reported interactors, such as Hnrnpa2b1, was maintained in our model (Buratti et al., 2005; D'Ambrogio et al., 2009). However, the absence of splicing factors (eg; Srsf7, Srsf4, Sf3b3) and the confirmed interruption of the interaction with Pabpc and Eif4a1 suggests potential contributions from dysregulated splicing, mRNA export and translation to ALS pathogenesis (Colombrita et al., 2012; Muller-McNicoll et al., 2016; Tollervey et al., 2011). Importantly, Pabpc is known to assemble in polysomes with other proteins implicated in translational dysregulation in ALS including Ataxin-2 and Matrin 3 (Boehringer et al., 2017; Nonhoff et al., 2007). Binding of TDP-43^{WT} to Pabpc may therefore be an important mediator of normal RNA processing in the cytoplasm of motor neurons (Ayala et al., 2011; Craig et al., 1998; He et al., 2014; Zhang et al., 2014). As we and others have shown, the M337V mutation is not in itself sufficient to interrupt the binding of Pabpc to TDP-43 (Freibaum et al., 2010). We suggest that a dysregulation in RNA metabolism may indirectly affect its interaction.

3.2. TDP-43^{M337V} alters stress response pathways

Oxidative stress increases with aging and is an important contributing factor to the pathology of neurodegenerative conditions and a potent trigger to stress granule formation (Guil et al., 2006). We found that in response to oxidative stress, TDP-43^{WT} interactions shift from networks regulating basal transcription and translation towards proteins involved in the endoplasmic reticulum-unfolded protein response, endosomal transport and extracellular exosome. This is in keeping with the protective response of general downregulation of translation in the cell, in which the capacity of TDP-43 to maintain interactions with stress response proteins and the formation of stress granules plays an important role (Kedersha and Anderson, 2002). The TDP-43$^{M337V/-}$ mutation in our model is associated with altered stress granule formation, a phenotype that has also been described in other ALS disease models, and may be mediated by the dynamic interaction of a wide repertoire of cytoplasmic RNA-binding proteins (Markmiller et al., 2018). Based on our study, we suggest that reduced binding between mutant TDP-43^{M337V} and Pabpc and Eif4a1, which are important for the initial assembly of stress granules, may be linked to impaired stress granule formation observed in TDP-43$^{M337V/-}$ mutant motor neurons, although demonstration of a direct effect of these interactors with stress granule formation is beyond the scope of this study. In response to stress, we found Grp78 bound preferentially to TDP-43^{WT}. Endoplasmic reticulum chaperones have been previously identified in association with ALS-related proteins, which suggests an important role of chaperones in maintaining protein homeostasis in motor neurons, possibly even within the cytoplasm (Atkin et al., 2006; Kikuchi et al., 2006; Walker et al., 2013). This is in line with the role of Grp78 in the assembly and disassembly of stress granules and conservation of the
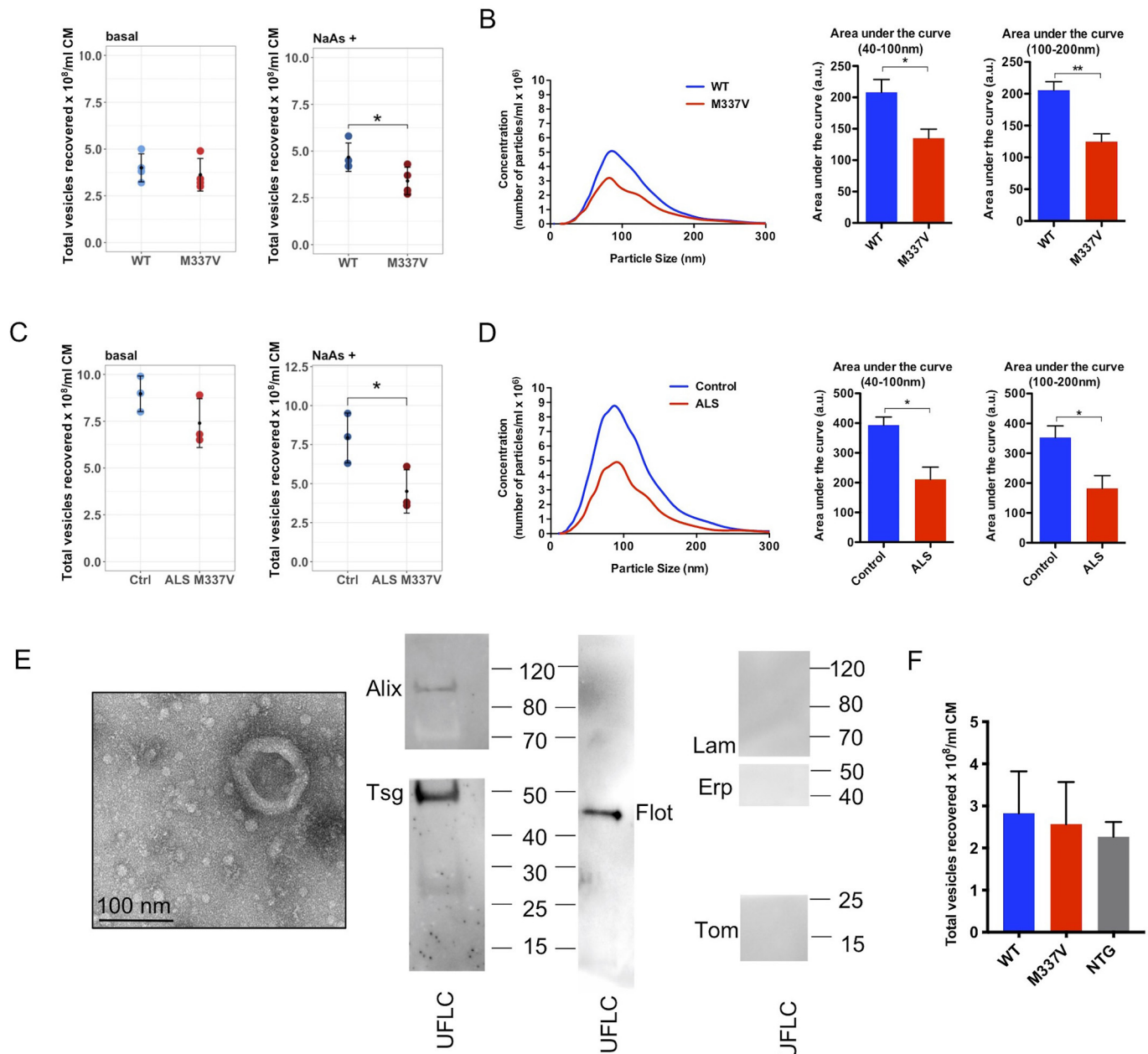
Fig. 6. In response to stress extracellular vesicle secretion is decreased in TDP-43$^{M337V/-}$ mouse and human ALS iPSC-derived MNs.
A Total number of EVs per ml condition media from TDP-43$^{M337V/-}$ and TDP-43$^{WT/-}$ mouse MNs in basal conditions, and in response to NaAsO$_2$ ($*p = 0.048$, n = 4 differentiations). B Size distribution of EVs given as total number per ml of conditioned media. C Total numbers of EVs from hiPSC-derived MNs from three healthy control lines and three clonal lines of an ALS patient with the M337V mutation. D The EV peak at 93 nm is decreased in ALS MNs and the area under the curve for exosomes (40–100 nm) and a mixed population of EVs (100–200 nm) (both $*p = 0.02$ and $p = 0.04$). E Transmission electron microscopy of EV extracts (scale bar 100 nm). EV extracts are immunoreactive for Alix at 96 kDa, Tsg101 at 48 kDa and Flotillin-1 at 48kDA. The immunoblot was negative for markers of the nucleus (Lamin B at 66 kDa), the endoplasmic reticulum (Erp44 at 38 kDa) and mitochondria (Tomm20 16 kDa). F The total number of EVs recovered from basal conditioned media is similar between TDP-43$^{WT/-}$ and TDP-43$^{M337V/-}$ (BAC)-transgenic MNs and non-transgenic MNs ($p = 0.71$, one-way ANOVA). Unpaired t-test; data are represented as mean ± SD. Abbreviations: EV, extracellular vesicle, hiPSC, human induced pluripotent stem-cells, MN, motor neuron.

integrity of stress granule components including Eif4a1 (Buchan, 2014; Matsumoto et al., 2011; Walker et al., 2013). In contrast, our proteomic data identified proteins in the TDP-43^{M337V} + NaAsO$_2$ interactome that are known to inhibit the formation of stress granules such as the chaperonin-containing T complex (CCT complex) (Jain et al., 2016; Leitner et al., 2012). In TDP-43 overexpression models, stress granule formation has often been reported as increased and associated with toxic aggregate formation, giving rise to the theory that stress granules seed TDP-43 aggregation (Chew et al., 2019; Li et al., 2013; Liu-Yesucevitz et al., 2010). However, a recent model in which TDP-43 proteinopathy is driven by optogenetic control has demonstrated that pathological aggregation of TDP-43 may occur independently of stress granule formation, albeit in the context of overexpression (Mann et al., 2019). Specific interactors gained by TDP-43^{M337V} in stress conditions such as Kelch-like proteins Klh15 and Kbtb4 and the loss of Grp78 interaction suggest involvement of the ubiquitin-proteasome pathway and activation of the unfolded protein response, which have been independently linked to ALS pathogenesis (Wang et al., 2010).

Consistent with the observation that knock-down of TDP-43 has a direct impact on endosomal trafficking (Schwenk et al., 2016), we

demonstrated interaction of TDP-43[WT] with proteins of the endosomal-extracellular vesicle secretion pathways. This included proteins such as Tmed9 which target vesicle transport to the plasma membrane for secretion. TDP-43[M337V/−] motor neurons, lack this interaction and showed a decrease in extracellular vesicle secretion compared to TDP-43[WT/−] motor neurons in response to stress. Importantly this was independently confirmed in human iPSC-derived motor neurons from a patient with the same mutation. This suggests that recognition of TDP-43[M337V] by the endosomal sorting complexes required for transport and secretion may be impaired in ALS neurons (Colombo et al., 2013). Whether this is due to a direct interaction such as with the Ras-related proteins (Aoki et al., 2017) or through an indirect mechanism, such as activation of the proteasome-ubiquitin pathway by TDP-43[M337V] (Iguchi et al., 2016), remains to be confirmed. Ultimately, reduced cytoplasmic trafficking of TDP-43 is likely to be a factor in the formation of cytoplasmic TDP-43 aggregates observed in 97% of ALS cases, and therefore could reflect a common therapeutic target upstream of protein aggregation (Chen-Plotkin et al., 2010; Winton et al., 2008).

In conclusion, in this study we observed that a single C-terminal mutation has multiple functional consequences, resulting in a pathological stress response which, under chronic conditions, might ultimately result in decreased survival of motor neurons. We focussed on the effect of mutant TDP-43 on protein-protein interactions, however we cannot rule out a contribution to pathology from differential TDP-43 binding to nucleic acids (Lim et al., 2016). Whether a loss of function of TDP-43 through impaired RNA-binding capacity, translation and splicing dysfunction or a toxic gain of function is a primary driver of ALS pathology is still a matter of debate (Lee et al., 2011; Ling et al., 2013). However, the results of this study support the hypothesis that multiple TDP-43 mediated pathways may be dysregulated in response to oxidative stress. This is also consistent with the concept of an age-dependent multiple hit model of neurodegeneration, in which loss of tolerance to inherent genetic mutations leads to the ultimate loss of cellular homeostasis in ALS.

4. Methods and materials

4.1. Motor neuron culture from mouse embryonic stem-cells

Mouse ESC-derived motor neurons were generated from the same ESC lines (IDG26.10–3) originally used in the creation of a bacterial artificial chromosome (BAC)-transgenic mouse model (RRID:IMSR_JAX:029266) carrying human YPet-tagged TDP-43[WT/−] or TDP-43[M337V/−] as previously described (Gordon et al., 2019; Wiese et al., 2010). We have recently described this model, in which human TDP-43 is expressed from a genomic insert integrated into the Rosa26 (Gt(ROSA26)Sor) locus of the mouse genome as a single stable copy, leading to expression levels below that of endogenous Tdp-43. Briefly, mESC were expanded on irradiated CF1 mouse embryonic fibroblasts (Gibco, RRID:CVCL_RB05) in Knockout DMEM (Invitrogen) containing 15% ESC-screened foetal bovine serum (ThermoFisher), 2 mM L-glutamine (Invitrogen), 0.01% MEM non-essential amino acids (Invitrogen), 1 ng/ml leukaemia inhibitory factor (Millipore), 0.01% EmbryoMax ESC qualified nucleosides (Millipore) and 0.1 mM 2-mercaptoethanol (Invitrogen). After 2 days embryoid bodies were separated from the feeder layer by treatment with 0.25% trypsin-EDTA (Gibco) and single cell suspension plated into 10 cm dishes (Corning) in 50% advanced DMEM/F-12 (Gibco), 50% Neurobasal medium (Gibco), 10% Knockout serum replacement (Gibco) and 2 mM L-glutamine and 0.01% Penicillin-streptomycin and 0.1 mM 2-mercaptoethanol (ADFNK medium). 1 μM retinoid acid (Merck) and 0.5 μM smoothened agonist (Merck) was added on day four and embryoid bodies were split on day six and eight. Embryoid bodies were collected and disaggregated on day nine. Embryoid bodies were collected and settled by gravity, washed with PBS and incubated with 2 ml of Accumax (Merck) for 10 min at 37 °C. Cells were filtered through a 40 μm cell strainer (Corning) and plated

on poly-L-ornithine (Merck) and laminin (Gibco) -coated plates in ADFNK medium plus retinoid acid, smoothened agonist and growth factors (10 ng/ml GDNF, 10 ng/ml BDNF, 25 ng/ml CNTF and 10 ng/ml NT-3; PeproTech). Mature motor neurons were ready for analysis after 2 days on day eleven. To examine the effect of oxidative stress, motor neurons were treated with 0.5 mM sodium arsenite (NaAsO₂; Merck) in growth media for 30 or 60 min. Cultured cells were then washed with PBS and either fixed with 4% PFA for immunocytochemistry or lysed with 1% NP-40 buffer for protein extraction and co-immunoprecipitation. Survival was assessed 4 h after 60 min of 0.5 mM NaAsO₂ treatment using an MTS Assay (Promega) relative to an untreated sample. The cultures were kept at 37 °C and 5% CO₂ for the duration of the experiments.

4.2. Human cellular models

HEK293T cells were transfected using Lipofectamine 2000 (Invitrogen) with full-length human TDP-43 with a C-terminal turboGFP-Tag (TDP-43 Human Tagged ORF Clone [Origene, CAT#: RG210639]) +/− M337V mutation inserted by site-directed mutagenesis (210,515, Agilent), TDP-43 empty control vector or N-terminal truncated TDP-43 'tdp43-EGFP construct 5' (a gift from Zuoshang Xu: Addgene plasmid #28198; http://n2t.net/addgene:28198; RRID:Addgene_28,198) (Yang et al., 2010).

All iPSC lines were reprogrammed from skin biopsy fibroblasts in the James Martin Stem-Cell Facility, University of Oxford, using standardized protocols as previously described (Dafinca et al., 2016). Human motor neurons (MNs) were differentiated from iPSCs for 30 days before conditioned media was retrieved for vesicle experiments, as previously described (Maury et al., 2015). Briefly, monolayers of iPSCs were induced in DMEM/F12/Neurobasal with N2 supplement (Life Technologies), B27 supplement (Life Technologies), ascorbic acid (0.5 μM), 2-mercaptoethanol (Life Technologies), 1 μM compound C (Millipore) and 3 μM Chir99021 (Bio-Techne) for 4 days. After 4 days in culture, 1 μM retinoic acid (Merck) and 500 nM smoothened agonist (Bio-Techne) were added to the medium. On day 5, Chir99021 and compound C were removed from the medium, and the cells were cultured for another 4–5 days. Neural precursors were then dissociated and plated at a low density for 7 days. The medium was supplemented with 10 ng/ml BDNF (Life Technologies), 10 ng/ml GDNF (Life Technologies), 10 μM DAPT and laminin (0.5 mg/ml). After 7 days, DAPT was removed from the medium, and the neurons were allowed to mature for another 2 weeks before functional experiments. A full description of the validation of this differentiation protocols has been described elsewhere (Dafinca et al., 2020).

4.3. Mass spectrometry and bioinformatics

For the study of the TDP-43 interactome, a total of 3 differentiations of mouse ESC-derived motor neurons harbouring human TDP-43[WT/−] or TDP-43[M337V/−] with or without 0.5 mM NaAsO₂ treatment for 60 min were generated. Cells were washed with PBS, incubated with 1% NP-40 buffer with 100 x HALT protease phosphatase inhibitor (ThermoFisher) for 5 min on ice, cells were scraped and centrifuged for 10 min at 10,000 ×g at 4 °C. 500 μg of protein lysate was used per immunoprecipitation reaction. YPet-tagged human TDP-43 was co-immunoprecipitated using GFP antibody-coated magnetic-agarose beads for 1 h (Chromotek, Germany). Beads were washed three times with wash buffer (10 mM Tris/Cl, 150 mM NaCl, 0.5 mM EDTA pH 7.5) and immunoprecipitated proteins bound to YPet-TDP-43 were directly digested with trypsin/lysC using in-StageTip method and frozen at −80 °C prior to elution for mass spectrometry following the manufacturer's instructions (Preomics, Germany). Interactors of human TDP-43 were identified by high performance liquid-chromatography tandem mass spectrometry (LC-MS/MS) using an Orbitrap Fusion Lumos mass spectrometer (ThermoScientific). Raw MS data were analysed using

Progenesis QI for Proteomics software v3.0 (Nonlinear Dynamics). MS/MS spectra were searched against the *Mus musculus* reference proteome (retrieved 15/11/2016) including the YPet-sequence using Mascot v2.5.1 (Matrix Science) allowing for a precursor mass tolerance of 10 ppm and a fragment ion tolerance of 0.5 Da. Carbamidomethylation on cysteines was defined as fixed modification and variable modification included deamidation on asparagine and glutamine and oxidation on methionine.

The peptide false discovery rate (FDR) was set at 1% and all peptides with an ion score higher than 20 were imported into Progenesis QIP. To further improve confidence in protein identification at least two peptides were required for protein identification, with 0.1% peptide FDR and 1% protein FDR. Protein abundance values were normalized to the median abundance of the 90% of proteins with the lowest variance across all runs and compared by *t*-test, with a FDR-adjusted *p*-value of ≤ 0.05 for significant differences and fold changes between TDP-43^{wt} and TDP-43^{M337V} interactors were calculated. For interactors where ion abundances were missing approximate quantification by peptide spectral count was used. A protein was defined as a putative interactor with ≥ 2 unique peptide spectra when 0 or 1 in the other interactome or ≥ 1 unique peptide spectral count when completely absent in the other interactome.

Gene ontology (GO) enrichment analysis was performed using TopGO (R-studio Version 1.1.383) applying a target-background approach at the gene level, with specific interactors of the TDP-43^{WT} (> 3 peptide spectral counts) or TDP-43^{M337V} $+/-$ NaAsO$_2$ interactome as the foreground list. The background list comprised all proteins identified over all twelve samples combined. Proteins of the interactomes significantly annotated to a GO term were determined by Fisher's exact test with a *p*-value < 0.05. The odds ratio (OR) indicates the ratio of significant identified proteins in the foreground list to the expected presence of proteins. Calculations were made to identify over-represented biological processes, cellular components and molecular functions. The top results are shown with the number of significant proteins ($p < 0.05$) identified in each GO term annotated using ggplot2 version 0.9.0 (R-studio Version 1.1.383, H. Wickham. ggplot2: Elegant Graphics for Data Analysis. Springer-Verlag New York, 2016). A visual network of protein-protein interactions was generated by STRING (consortium 2019) utilized through Cytoscape v3.3.0 selecting *Mus musculus* organism and high confidence interactions.

4.4. Immunohistochemistry and microscopy

Cells cultured on glass coverslips were fixed with 4% PFA-PBS for 15 min and blocked with 5% normal donkey serum with 0.1% Triton X-100 for 1 h at room temperature (RT). The cells were incubated overnight with primary antibody diluted in 1% donkey serum (mouse or rabbit anti-Tuj1 (Covance, 1:1000), mouse anti-Islet1 (40.2D6-A, Developmental Studies Hybridoma Bank, 1:1000), goat anti-ChAT (ab144P, Millipore, 1:500), rabbit anti-GFP (Invitrogen, 10,474,172, 1:1000), rabbit anti-cleaved-caspase 3 (9661, Cell Signaling, 1:500), rabbit anti-PABPc protein (ab21060, Abcam, 1:1000). After washing with 0.1% Triton-X/PBS for 10 min three times the samples were incubated with Alexa Fluor 488 or Alexa Fluor 568 conjugated donkey anti-rabbit, anti-mouse or anti-goat secondary antibodies (Life Technologies, 1:1000) for 1 h at RT. After washing with 0.1% Triton-X/PBS for 10 min twice, nuclei were stained with 4′,6-Diamidino-2-Phenylindole (DAPI) for 10 min. Coverslips were mounted and fluorescence was visualized using a confocal microscope Zeiss LSM. Cells from six randomly chosen-fields were counted and percentage of total cells (at least 60 total cells) averaged for each differentiation. Statistical analysis compared average values from each differentiation (total differentiations per experiment $n = 3$).

4.5. Stress granule analysis

Images for stress granules were acquired with an $63\times$ objective and 10.24 resolution. Images were produced with z-stacks (0.25 μm interval) with a scan area 1.0–1.5 zoom in Zen lite 2012 software (Zeiss) and z-projected using Fiji version 1.0 of ImageJ. The number of cells with stress granules were counted and given as percentage of the total cell count. The number and area of stress granules per motor neuron were assessed by an automated macro analysis programmed for the recognition of stress granules of the size from 100nm^2 to 1.5μm^2 (Fiji version 1.0 of ImageJ).

4.6. Immunoprecipitation and immunoblotting

For Co-immunoprecipitations cells were lysed with 1% NP-40 buffer as described above. 1000 - 2000 μg of protein lysate was used per immunoprecipitation reaction. For RNase treatment.

protein extracts were incubated with either vehicle (10 mM Tris-HCl, pH 7.5, 15 mM NaCl) or 330 μg of RNAse A (Roche) for 10 min at 37 °C on a shaker. After samples have been cooled on ice followed by co-immunoprecipitation. YPet-tagged human TDP-43 was co-immunoprecipitated using 25 μl of GFP antibody-coated magnetic-agarose beads per sample (Chromotek). turboGFP-tagged human TDP-43 was co-immunoprecipitated using 25 μl of turboGFP (tGFP) antibody-coated magnetic-agarose beads per sample (Chromotek). IP-eluates were directly suspended in 30 μl 2× LDS sample buffer and 7.5 μl of 4× LDS buffer was added to 19 μl of the supernatants. All samples were supplemented with 10× reducing agent (Invitrogen) and boiled at 95 °C for 10 min. Sample were run on a 4–12% gradient precast gel (Invitrogen) at 135 V for 2.5 h in MOPS running buffer (Invitrogen). Membranes were blocked in TBS protein free blocking buffer (ThermoFisher) and incubated overnight with primary antibody, as follows: rabbit anti-GFP (10,474,172, Invitrogen, 1:1000), rabbit ant-turboGFP (PA5–22688, Invitrogen, 1:1000) rabbit anti-PABPc (ab21060, Abcam, 1:1000), rabbit anti-TDP-43 (10782–2-AP, Proteintech, 1:1000), rabbit anti-Eif4a1 (2490, Cell signaling, 1:1000), rabbit anti-Tmed9 (SAB2700249, Merck, 1:1000), rabbit anti-Grp78 (ab21685, Abcam, 1:1000), diluted in protein free blocking buffer followed by respective secondary antibodies (Novus Biologicals, 1:10000). ECL (GE Healthcare, RPN2232) signal was visualized using the BioRad ChemiDoc imaging system. Signal intensity was quantified using the Fiji version 1.0 of ImageJ. After immunoblotting the immunoreactivity of the co-immunoprecipitated protein was semi-quantified relative to the normalized immunoreactivity of the immunoprecipitated bait protein after stripping the membrane.

4.7. Ultrafiltration liquid chromatography and extracellular vesicle characterization

Extracellular vesicle (EV) characterizations were performed in EV-depleted media prepared by ultracentrifugation for respective cell culture mediums centrifuged at 120,000 $\times g$ for 18 h (Beckman Coulter, Optima MAX-XP Ultracentrifuge). Motor neuron cultures were plated at equal density on a 6-well plate. On day eleven motor neuron cultures were exposed to EV-depleted conditioned media $+/-$ 0.5 mM NaAsO$_2$ for 60 min, the media was then collected and immediately frozen at -80 °C. Collected media was then defrosted on ice and centrifuged and following filtration (0.22 μm), samples were filtered using Amicon Ultra-15,100 kDa molecular weight cut-off (MWCO) centrifugal filters (Merck Millipore) at 3500 $\times g$ for 8 min, washed with PBS and centrifuged at 3500 $\times g$ for 4 min. Retentate volume was adjusted to 800 μL with PBS, injected into a 24 ml size exclusion column packed with sepharose 4 fastflow (mean particle size 90 μm, exclusion limit 3 $\times 10^7$) and eluted with 40 ml PBS at 0.5 ml per minute using an AKTA pure chromatography system (GE Life Sciences). Two millilitre fractions were collected from six to 40 ml elution volume. Extracellular size

distribution and concentration was ascertained using nanoparticle tracking analysis (NTA) using a NanoSight NS500 (Malvern Ltd) and NTA 2.3 software. Size distribution was averaged across three 30 s recordings per sample (Thompson et al., 2018). Immunoblotting for positive markers rabbit anti-Alix (ab186429, Abcam, 1:1000), rabbit anti-TSG101 (ab125011, Abcam, 1:500) and mouse anti-Flotillin-1 (Novus Biologicals, 1:1000), as well as negative markers rabbit anti-Tomm-20 (ab56783, Abcam, 1:1000), rabbit anti-Erp44 (SAB1410402, Merck, 1:1000) and mouse anti-Lamin B (X223, Invitrogen, 1:1000) was done by collecting EV containing fractions 2 and 3 in ultracentrifuge tubes and centrifuge for 120 000 $\times g$ for 2 h at 4 °C. Supernatant was collected as negative control and the vesicle pellet washed with PBS and centrifuged 120 000 $\times g$ for 2 h again. The vesicle pellet was then dissolved in 4xLDS sample buffer.

4.8. Transmission electron microscopy

10 μL of EV solution was applied to freshly glow-discharged carbon-coated 200 mesh copper grids for 2 min, blotted with filter paper and stained with 2% uranyl acetate for 10 s, blotted and air dried. Grids were imaged in a FEI Tecnai 12 transmission electron microscope at 120 kV using a Gatan OneView CMOS camera. Particle size was measured using ImageJ v1.50i (National Institutes of Health, USA).

4.9. Statistical analysis

Proteomic analysis is detailed above. Data are presented as mean and standard deviation and unpaired t-test was used to assess significant differences ($p < 0.05$). One-way ANOVA analysis was used to determine statistical differences between three or more groups. The exact value of the number of replicates and the statistical test and result are given in the figure legends. Statistical analysis was carried out using R-Studio and GraphPad Prism 7 (version7b, 2016).

Declaration of competing interest

The authors declare that they have no conflicts of interest.

Availability of data and materials

Protein interaction AP-MS data PRIDE PXD010354 (https://www.ebi.ac.uk/pride/archive/projects/PXD010354/files).

Appendix A. Supplementary data

Supplementary data to this article can be found online at https://doi.org/10.1016/j.nbd.2020.105050.

References

Aoki, Y., Manzano, R., Lee, Y., Dafinca, R., Aoki, M., Douglas, A.G.L., Varela, M.A., Sathyaprakash, C., Scaber, J., Barbagallo, P., Vader, P., Mager, I., Ezzat, K., Turner, M.R., Ito, N., Gasco, S., Ohbayashi, N., El Andaloussi, S., Takeda, S., Fukuda, M., Talbot, K., Wood, M.J.A., 2017. C9orf72 and RAB7L1 regulate vesicle trafficking in amyotrophic lateral sclerosis and frontotemporal dementia. Brain 140 (4), 887–897. https://doi.org/10.1093/brain/awx024.

Atkin, J.D., Farg, M.A., Turner, B.J., Tomas, D., Lysaght, J.A., Nunan, J., Rembach, A., Nagley, P., Beart, P.M., Cheema, S.S., Horne, M.K., 2006. Induction of the unfolded protein response in familial amyotrophic lateral sclerosis and association of protein-disulfide isomerase with superoxide dismutase 1. J. Biol. Chem. 281 (40), 30152–30165. https://doi.org/10.1074/jbc.M603393200.

Ayala, Y.M., De Conti, L., Avendano-Vazquez, S.E., Dhir, A., Romano, M., D'Ambrogio, A., Tollervey, J., Ule, J., Baralle, M., Buratti, E., Baralle, F.E., 2011. TDP-43 regulates its mRNA levels through a negative feedback loop. EMBO J. 30 (2), 277–288. https://doi.org/10.1038/emboj.2010.310.

Blasco, H., Bernard-Marissal, N., Vourc'h, P., Guettard, Y.O., Sunyach, C., Augereau, O., Khederchah, J., Mouzat, K., Antar, C., Gordon, P.H., Veyrat-Durebex, C., Besson, G., Andersen, P.M., Salachas, F., Meininger, V., Camu, W., Pettmann, B., Andres, C.R., Corcia, P., French, A.L.S.S.G., 2013. A rare motor neuron deleterious missense mutation in the DPYSL3 (CRMP4) gene is associated with ALS. Hum. Mutat. 34 (7), 953–960. https://doi.org/10.1002/humu.22329.

Blokhuis, A.M., Koppers, M., Groen, E.J., van den Heuvel, D.M., Dini Modigliani, S., Anink, J.J., Fumoto, K., van Diggelen, F., Snelting, A., Sodaar, P., Verheijen, B.M., Demmers, J.A., Veldink, J.H., Aronica, E., Bozzoni, I., den Hertog, J., van den Berg, L.H., Pasterkamp, R.J., 2016. Comparative interactomics analysis of different ALS-associated proteins identifies converging molecular pathways. Acta Neuropathol. 132 (2), 175–196. https://doi.org/10.1007/s00401-016-1575-8.

Boehringer, A., Garcia-Mansfield, K., Singh, G., Bakkar, N., Pirrotte, P., Bowser, R., 2017. ALS associated mutations in matrin 3 alter protein-protein interactions and impede mRNA nuclear export. Sci. Rep. 7 (1), 14529. https://doi.org/10.1038/s41598-017-14924-6.

Brettschneider, J., Del Tredici, K., Toledo, J.B., Robinson, J.L., Irwin, D.J., Grossman, M., Suh, E., Van Deerlin, V.M., Wood, E.M., Baek, Y., Kwong, L., Lee, E.B., Elman, L., McCluskey, L., Fang, L., Feldengut, S., Ludolph, A.C., Lee, V.M., Braak, H., Trojanowski, J.Q., 2013. Stages of pTDP-43 pathology in amyotrophic lateral sclerosis. Ann. Neurol. 74 (1), 20–38. https://doi.org/10.1002/ana.23937.

Buchan, J.R., 2014. mRNP granules. Assembly, function, and connections with disease. RNA Biol. 11 (8), 1019–1030. https://doi.org/10.4161/15476286.2014.972208.

Buratti, E., Baralle, F.E., 2008. Multiple roles of TDP-43 in gene expression, splicing regulation, and human disease. Front. Biosci. 13, 867–878.

Buratti, E., Brindisi, A., Giombi, M., Tisminetzky, S., Ayala, Y.M., Baralle, F.E., 2005. TDP-43 binds heterogeneous nuclear ribonucleoprotein A/B through its C-terminal tail: an important region for the inhibition of cystic fibrosis transmembrane conductance regulator exon 9 splicing. J. Biol. Chem. 280 (45), 37572–37584. https://doi.org/10.1074/jbc.M505557200.

Chen-Plotkin, A.S., Lee, V.M., Trojanowski, J.Q., 2010. TAR DNA-binding protein 43 in neurodegenerative disease. Nat. Rev. Neurol. 6 (4), 211–220. https://doi.org/10.1038/nrneurol.2010.18.

Chew, J., Cook, C., Gendron, T.F., Jansen-West, K., Del Rosso, G., Daughrity, L.M., Castanedes-Casey, M., Kurti, A., Stankowski, J.N., Disney, M., Rothstein, J.D., Dickson, D.W., Fryer, J.D., Zhang, Y.J., Petrucelli, L., 2019. Aberrant deposition of stress granule-resident proteins linked to C9orf72-associated TDP-43 proteinopathy. Mol. Neurodegener. 14 (1), 9. https://doi.org/10.1186/s13024-019-0310-z.

Colombo, M., Moita, C., van Niel, G., Kowal, J., Vigneron, J., Benaroch, P., Manel, N., Moita, L.F., Thery, C., Raposo, G., 2013. Analysis of ESCRT functions in exosome biogenesis, composition and secretion highlights the heterogeneity of extracellular vesicles. J. Cell Sci. 126 (Pt 24), 5553–5565. https://doi.org/10.1242/jcs.128868.

Colombrita, C., Zennaro, E., Fallini, C., Weber, M., Sommacal, A., Buratti, E., Silani, V., Ratti, A., 2009. TDP-43 is recruited to stress granules in conditions of oxidative insult. J. Neurochem. 111 (4), 1051–1061. https://doi.org/10.1111/j.1471-4159.2009.06383.x.

Colombrita, C., Onesto, E., Megiorni, F., Pizzuti, A., Baralle, F.E., Buratti, E., Silani, V., Ratti, A., 2012. TDP-43 and FUS RNA-binding proteins bind distinct sets of cytoplasmic messenger RNAs and differently regulate their post-transcriptional fate in motoneuron-like cells. J. Biol. Chem. 287 (19), 15635–15647. https://doi.org/10.1074/jbc.M111.333450.

Conicella, A.E., Zerze, G.H., Mittal, J., Fawzi, N.L., 2016. ALS mutations disrupt phase separation mediated by alpha-helical structure in the TDP-43 low-complexity C-terminal domain. Structure 24 (9), 1537–1549. https://doi.org/10.1016/j.str.2016.07.007.

Craig, A.W., Haghighat, A., Yu, A.T., Sonenberg, N., 1998. Interaction of polyadenylate-binding protein with the eIF4G homologue PAIP enhances translation. Nature 392 (6675), 520–523. https://doi.org/10.1038/33198.

Dafinca, R., Scaber, J., Ababneh, N., Lalic, T., Weir, G., Christian, H., Vowles, J., Douglas, A.G., Fletcher-Jones, A., Browne, C., Nakanishi, M., Turner, M.R., Wade-Martins, R., Cowley, S.A., Talbot, K., 2016. C9orf72 Hexanucleotide expansions are associated with altered endoplasmic reticulum calcium homeostasis and stress granule formation in induced pluripotent stem cell-derived neurons from patients with amyotrophic lateral sclerosis and frontotemporal dementia. Stem Cells 34 (8), 2063–2078. https://doi.org/10.1002/stem.2388.

Dafinca, R., Barbagallo, P., Farrimond, L., Candalija, A., Scaber, J., Ababneh, N.A., Sathyaprakash, C., Vowles, J., Cowley, S.A., Talbot, K., 2020. Impairment of mitochondrial calcium buffering links mutations in C9ORF72 and TARDBP in iPS-derived motor neurons from patients with ALS/FTD. Stem Cell Rep. 14 (5), 892–908. https://doi.org/10.1016/j.stemcr.2020.03.023.

D'Ambrogio, A., Buratti, E., Stuani, C., Guarnaccia, C., Romano, M., Ayala, Y.M., Baralle, F.E., 2009. Functional mapping of the interaction between TDP-43 and hnRNP A2 in vivo. Nucleic Acids Res. 37 (12), 4116–4126. https://doi.org/10.1093/nar/gkp342.

Freibaum, B.D., Chitta, R.K., High, A.A., Taylor, J.P., 2010. Global analysis of TDP-43 interacting proteins reveals strong association with RNA splicing and translation machinery. J. Proteome Res. 9 (2), 1104–1120. https://doi.org/10.1021/pr901076y.

Gordon, D., Dafinca, R., Scaber, J., Alegre-Abarrategui, J., Farrimond, L., Scott, C., Biggs, D., Kent, L., Oliver, P.L., Davies, B., Ansorge, O., Wade-Martins, R., Talbot, K., 2019. Single-copy expression of an amyotrophic lateral sclerosis-linked TDP-43 mutation (M337V) in BAC transgenic mice leads to altered stress granule dynamics and

progressive motor dysfunction. Neurobiol. Dis. 121, 148–162. https://doi.org/10.1016/j.nbd.2018.09.024.

Guil, S., Long, J.C., Caceres, J.F., 2006. hnRNP A1 relocalization to the stress granules reflects a role in the stress response. Mol. Cell. Biol. 26 (15), 5744–5758. https://doi.org/10.1128/MCB.00224-06.

Harrison, A.F., Shorter, J., 2017. RNA-binding proteins with prion-like domains in health and disease. Biochem. J. 474 (8), 1417–1438. https://doi.org/10.1042/BCJ20160499.

He, F., Krans, A., Freibaum, B.D., Taylor, J.P., Todd, P.K., 2014. TDP-43 suppresses CGG repeat-induced neurotoxicity through interactions with HnRNP A2/B1. Hum. Mol. Genet. 23 (19), 5036–5051. https://doi.org/10.1093/hmg/ddu216.

Iguchi, Y., Eid, L., Parent, M., Soucy, G., Bareil, C., Riku, Y., Kawai, K., Takagi, S., Yoshida, M., Katsuno, M., Sobue, G., Julien, J.P., 2016. Exosome secretion is a key pathway for clearance of pathological TDP-43. Brain 139 (Pt 12), 3187–3201. https://doi.org/10.1093/brain/aww237.

Jain, S., Wheeler, J.R., Walters, R.W., Agrawal, A., Barsic, A., Parker, R., 2016. ATPase-modulated stress granules contain a diverse proteome and substructure. Cell 164 (3), 487–498. https://doi.org/10.1016/j.cell.2015.12.038.

Kato, M., Han, T.W., Xie, S., Shi, K., Du, X., Wu, L.C., Mirzaei, H., Goldsmith, E.J., Longgood, J., Pei, J., Grishin, N.V., Frantz, D.E., Schneider, J.W., Chen, S., Li, L., Sawaya, M.R., Eisenberg, D., Tycko, R., McKnight, S.L., 2012. Cell-free formation of RNA granules: low complexity sequence domains form dynamic fibers within hydrogels. Cell 149 (4), 753–767. https://doi.org/10.1016/j.cell.2012.04.017.

Kedersha, N., Anderson, P., 2002. Stress granules: sites of mRNA triage that regulate mRNA stability and translatability. Biochem. Soc. Trans. 30 (Pt 6), 963–969. https://doi.org/10.1042/bst0300963.

Kikuchi, H., Almer, G., Yamashita, S., Guegan, C., Nagai, M., Xu, Z., Sosunov, A.A., McKhann 2nd, G.M., Przedborski, S., 2006. Spinal cord endoplasmic reticulum stress associated with a microsomal accumulation of mutant superoxide dismutase-1 in an ALS model. Proc. Natl. Acad. Sci. U. S. A. 103 (15), 6025–6030. https://doi.org/10.1073/pnas.0509227103.

Kimball, S.R., Horetsky, R.L., Ron, D., Jefferson, L.S., Harding, H.P., 2003. Mammalian stress granules represent sites of accumulation of stalled translation initiation complexes. Am. J. Phys. Cell Phys. 284 (2), C273–C284. https://doi.org/10.1152/ajpcell.00314.2002.

Lee, E.B., Lee, V.M., Trojanowski, J.Q., 2011. Gains or losses: molecular mechanisms of TDP43-mediated neurodegeneration. Nat. Rev. Neurosci. 13 (1), 38–50. https://doi.org/10.1038/nrn3121.

Leitner, A., Joachimiak, L.A., Bracher, A., Monkemeyer, L., Walzthoeni, T., Chen, B., Pechmann, S., Holmes, S., Cong, Y., Ma, B., Ludtke, S., Chiu, W., Hartl, F.U., Aebersold, R., Frydman, J., 2012. The molecular architecture of the eukaryotic chaperonin TRiC/CCT. Structure 20 (5), 814–825. https://doi.org/10.1016/j.str.2012.03.007.

Li, Y.R., King, O.D., Shorter, J., Gitler, A.D., 2013. Stress granules as crucibles of ALS pathogenesis. J. Cell Biol. 201 (3), 361–372. https://doi.org/10.1083/jcb.201302044.

Li, Y., Collins, M., An, J., Geiser, R., Tegeler, T., Tsantilas, K., Garcia, K., Pirrotte, P., Bowser, R., 2016. Immunoprecipitation and mass spectrometry defines an extensive RBM45 protein-protein interaction network. Brain Res. 1647, 79–93. https://doi.org/10.1016/j.brainres.2016.02.047.

Lim, L., Wei, Y., Lu, Y., Song, J., 2016. ALS-causing mutations significantly perturb the self-assembly and interaction with nucleic acid of the intrinsically disordered prion-like domain of TDP-43. PLoS Biol. 14 (1), e1002338. https://doi.org/10.1371/journal.pbio.1002338.

Ling, S.C., Albuquerque, C.P., Han, J.S., Lagier-Tourenne, C., Tokunaga, S., Zhou, H., Cleveland, D.W., 2010. ALS-associated mutations in TDP-43 increase its stability and promote TDP-43 complexes with FUS/TLS. Proc. Natl. Acad. Sci. U. S. A. 107 (30), 13318–13323. https://doi.org/10.1073/pnas.1008227107.

Ling, S.C., Polymenidou, M., Cleveland, D.W., 2013. Converging mechanisms in ALS and FTD: disrupted RNA and protein homeostasis. Neuron 79 (3), 416–438. https://doi.org/10.1016/j.neuron.2013.07.033.

Liu-Yesucevitz, L., Bilgutay, A., Zhang, Y.J., Vanderweyde, T., Citro, A., Mehta, T., Zaarur, N., McKee, A., Bowser, R., Sherman, M., Petrucelli, L., Wolozin, B., 2010. Tar DNA binding protein-43 (TDP-43) associates with stress granules: analysis of cultured cells and pathological brain tissue. PLoS One 5 (10), e13250. https://doi.org/10.1371/journal.pone.0013250.

Mann, J.R., Gleixner, A.M., Mauna, J.C., Gomes, E., DeChellis-Marks, M.R., Needham, P.G., Copley, K.E., Hurtle, B., Portz, B., Pyles, N.J., Guo, L., Calder, C.B., Wills, Z.P., Pandey, U.B., Kofler, J.K., Brodsky, J.L., Thathiah, A., Shorter, J., Donnelly, C.J., 2019. RNA binding antagonizes neurotoxic phase transitions of TDP-43. Neuron. https://doi.org/10.1016/j.neuron.2019.01.048.

Markmiller, S., Soltanieh, S., Server, K.L., Mak, R., Jin, W., Fang, M.Y., Luo, E.C., Krach, F., Yang, D., Sen, A., Fulzele, A., Wozniak, J.M., Gonzalez, D.J., Kankel, M.W., Gao, F.B., Bennett, E.J., Lecuyer, E., Yeo, G.W., 2018. Context-dependent and disease-specific diversity in protein interactions within stress granules. Cell 172 (3), 590–604 e513. https://doi.org/10.1016/j.cell.2017.12.032.

Matsumoto, K., Minami, M., Shinozaki, F., Suzuki, Y., Abe, K., Zenno, S., Matsumoto, S., Minami, Y., 2011. Hsp90 is involved in the formation of P-bodies and stress granules. Biochem. Biophys. Res. Commun. 407 (4), 720–724. https://doi.org/10.1016/j.bbrc.2011.03.088.

Maury, Y., Come, J., Piskorowski, R.A., Salah-Mohellibi, N., Chevaleyre, V., Peschanski, M., Martinat, C., Nedelec, S., 2015. Combinatorial analysis of developmental cues efficiently converts human pluripotent stem cells into multiple neuronal subtypes. Nat. Biotechnol. 33 (1), 89–96. https://doi.org/10.1038/nbt.3049.

McKee, A.C., Cairns, N.J., Dickson, D.W., Folkerth, R.D., Keene, C.D., Litvan, I., Perl, D.P., Stein, T.D., Vonsattel, J.P., Stewart, W., Tripodis, Y., Crary, J.F., Bieniek, K.F., Dams-O'Connor, K., Alvarez, V.E., Gordon, W.A., Group, T.C., 2016. The first NINDS/NIBIB consensus meeting to define neuropathological criteria for the diagnosis of chronic traumatic encephalopathy. Acta Neuropathol. 131 (1), 75–86. https://doi.org/10.1007/s00401-015-1515-z.

Muller-McNicoll, M., Botti, V., de Jesus Domingues, A.M., Brandl, H., Schwich, O.D., Steiner, M.C., Curk, T., Poser, I., Zarnack, K., Neugebauer, K.M., 2016. SR proteins are NXF1 adaptors that link alternative RNA processing to mRNA export. Genes Dev. 30 (5), 553–566. https://doi.org/10.1101/gad.276477.115.

Nelson, P.T., Dickson, D.W., Trojanowski, J.Q., Jack, C.R., Boyle, P.A., Arfanakis, K., Rademakers, R., Alafuzoff, I., Attems, J., Brayne, C., Coyle-Gilchrist, I.T.S., Chui, H.C., Fardo, D.W., Flanagan, M.E., Halliday, G., Hokkanen, S.R.K., Hunter, S., Jicha, G.A., Katsumata, Y., Kawas, C.H., Keene, C.D., Kovacs, G.G., Kukull, W.A., Levey, A.I., Makkinejad, N., Montine, T.J., Murayama, S., Murray, M.E., Nag, S., Rissman, R.A., Seeley, W.W., Sperling, R.A., White Iii, C.L., Yu, L., Schneider, J.A., 2019. Limbic-predominant age-related TDP-43 encephalopathy (LATE): consensus working group report. Brain. https://doi.org/10.1093/brain/awz099.

Neumann, M., Sampathu, D.M., Kwong, L.K., Truax, A.C., Micsenyi, M.C., Chou, T.T., Bruce, J., Schuck, T., Grossman, M., Clark, C.M., McCluskey, L.F., Miller, B.L., Masliah, E., Mackenzie, I.R., Feldman, H., Feiden, W., Kretzschmar, H.A., Trojanowski, J.Q., Lee, V.M., 2006. Ubiquitinated TDP-43 in frontotemporal lobar degeneration and amyotrophic lateral sclerosis. Science 314 (5796), 130–133. doi:314/5796/130 [pii]. https://doi.org/10.1126/science.1134108.

Nonhoff, U., Ralser, M., Welzel, F., Piccini, I., Balzereit, D., Yaspo, M.L., Lehrach, H., Krobitsch, S., 2007. Ataxin-2 interacts with the DEAD/H-box RNA helicase DDX6 and interferes with P-bodies and stress granules. Mol. Biol. Cell 18 (4), 1385–1396. https://doi.org/10.1091/mbc.e06-12-1120.

Ou, S.H., Wu, F., Harrich, D., Garcia-Martinez, L.F., Gaynor, R.B., 1995. Cloning and characterization of a novel cellular protein, TDP-43, that binds to human immunodeficiency virus type 1 TAR DNA sequence motifs. J. Virol. 69 (6), 3584–3596.

Schwenk, B.M., Hartmann, H., Serdaroglu, A., Schludi, M.H., Hornburg, D., Meissner, F., Orozco, D., Colombo, A., Tahirovic, S., Michaelsen, M., Schreiber, F., Haupt, S., Peitz, M., Brustle, O., Kupper, C., Klopstock, T., Otto, M., Ludolph, A.C., Arzberger, T., Kuhn, P.H., Edbauer, D., 2016. TDP-43 loss of function inhibits endosomal trafficking and alters trophic signaling in neurons. EMBO J. 35 (21), 2350–2370. https://doi.org/10.15252/embj.201694221.

Shaw, P.J., Ince, P.G., Falkous, G., Mantle, D., 1995. Oxidative damage to protein in sporadic motor neuron disease spinal cord. Ann. Neurol. 38 (4), 691–695. https://doi.org/10.1002/ana.410380424.

Sleigh, J.N., Tosolini, A.P., Gordon, D., Devoy, A., Fratta, P., Fisher, E.M.C., Talbot, K., Schiavo, G., 2020. Mice carrying ALS mutant TDP-43, but not mutant FUS, display in vivo defects in axonal transport of Signaling endosomes. Cell Rep. 30 (11), 3655–3662 e3652. https://doi.org/10.1016/j.celrep.2020.02.078.

Sreedharan, J., Blair, I.P., Tripathi, V.B., Hu, X., Vance, C., Rogelj, B., Ackerley, S., Durnall, J.C., Williams, K.L., Buratti, E., Baralle, F., de Belleroche, J., Mitchell, J.D., Leigh, P.N., Al-Chalabi, A., Miller, C.C., Nicholson, G., Shaw, C.E., 2008. TDP-43 mutations in familial and sporadic amyotrophic lateral sclerosis. Science 319 (5870), 1668–1672. https://doi.org/10.1126/science.1154584.

Thery, C., Amigorena, S., Raposo, G., Clayton, A., 2006. Isolation and characterization of exosomes from cell culture supernatants and biological fluids. In: Curr Protoc Cell Biol, https://doi.org/10.1002/0471143030.cb0322s30. Chapter 3:Unit 3 22.

Thompson, A.G., Gray, E., Mager, I., Fischer, R., Thezenas, M.L., Charles, P.D., Talbot, K., El Andaloussi, S., Kessler, B.M., Wood, M., Turner, M.R., 2018. UFLC-derived CSF extracellular vesicle origin and proteome. Proteomics 18 (24), e1800257. https://doi.org/10.1002/pmic.201800257.

Tollervey, J.R., Curk, T., Rogelj, B., Briese, M., Cereda, M., Kayikci, M., Konig, J., Hortobagyi, T., Nishimura, A.L., Zupunski, V., Patani, R., Chandran, S., Rot, G., Zupan, B., Shaw, C.E., Ule, J., 2011. Characterizing the RNA targets and position-dependent splicing regulation by TDP-43. Nat. Neurosci. 14 (4), 452–458. https://doi.org/10.1038/nn.2778.

Walker, A.K., Soo, K.Y., Sundaramoorthy, V., Parakh, S., Ma, Y., Farg, M.A., Wallace, R.H., Crouch, P.J., Turner, B.J., Horne, M.K., Atkin, J.D., 2013. ALS-associated TDP-43 induces endoplasmic reticulum stress, which drives cytoplasmic TDP-43 accumulation and stress granule formation. PLoS One 8 (11), e81170. https://doi.org/10.1371/journal.pone.0081170.

Wang, X., Fan, H., Ying, Z., Li, B., Wang, H., Wang, G., 2010. Degradation of TDP-43 and its pathogenic form by autophagy and the ubiquitin-proteasome system. Neurosci. Lett. 469 (1), 112–116. https://doi.org/10.1016/j.neulet.2009.11.055.

Wiese, S., Herrmann, T., Drepper, C., Jablonka, S., Funk, N., Klausmeyer, A., Rogers, M.L., Rush, R., Sendtner, M., 2010. Isolation and enrichment of embryonic mouse motoneurons from the lumbar spinal cord of individual mouse embryos. Nat. Protoc. 5 (1), 31–38. https://doi.org/10.1038/nprot.2009.193.

Winton, M.J., Igaz, L.M., Wong, M.M., Kwong, L.K., Trojanowski, J.Q., Lee, V.M., 2008. Disturbance of nuclear and cytoplasmic TAR DNA-binding protein (TDP-43) induces disease-like redistribution, sequestration, and aggregate formation. J. Biol. Chem. 283 (19), 13302–13309. https://doi.org/10.1074/jbc.M800342200.

Yang, C., Tan, W., Whittle, C., Qiu, L., Cao, L., Akbarian, S., Xu, Z., 2010. The C-terminal TDP-43 fragments have a high aggregation propensity and harm neurons by a dominant-negative mechanism. PLoS One 5 (12), e15878. https://doi.org/10.1371/journal.pone.0015878.

Zhang, T., Baldie, G., Periz, G., Wang, J., 2014. RNA-processing protein TDP-43 regulates FOXO-dependent protein quality control in stress response. PLoS Genet. 10 (10), e1004693. https://doi.org/10.1371/journal.pgen.1004693.